

Thermochemical etching of polycrystalline diamond films by nickel

Ondrej Szabó*, Gabriel Vanko, Kateřina Aubrechtová Dragounová, Štěpán Potocký, Alexander Kromka

Institute of Physics of the Czech Academy of Sciences, Cukrovarnická 10/112, 162 00 Prague 6, Czech Republic

*Corresponding author: szabo@fzu.cz

Abstract

This study investigates the deep etching characteristics of microcrystalline diamond films using a Ni-catalyzed thermochemical process conducted at different temperatures (750-900°C) and gas compositions. Under H₂ microwave plasma conditions, minimal etching was observed beneath the Ni mask. Although introducing CO₂ into the gas mixture enhanced the etching rate by factors of 2-3, it resulted in non-selective etching of unmasked regions.

Changing to water vapor conditions led to superior etching selectivity, though the process was still pressure-dependent. At low pressure (65 mbar), catalytic etching achieved a maximum depth of 5-6 µm due to saturated graphitization around Ni. This limitation was overcome by increasing atmospheric pressure, enabling the formation of depth structures up to 20 µm with an etching rate of 45 µm/h. Temperature-dependent studies were conducted to evaluate the etch profile evolution. Using a 200 nm thick Ni mask at 900°C under atmospheric pressure conditions, we achieved highly anisotropic etching with vertical sidewalls, contrasting with the sloped profiles typically observed in single-crystal diamond etching. This technology presents a cost-effective alternative to conventional dry plasma etching processes for fabricating complex 3D structures.

Keywords:

Thermochemical process, polycrystalline diamond, catalytic graphitization, deep etching, hot water vapor, SEM.

1. Introduction

Diamond possesses extraordinary physical and electronic properties, including optical, thermal, and mechanical characteristics that make it invaluable across diverse applications. The unique combination of properties has established diamond as a progressive material in electronics [1], photonics, optics, opto-mechanics, and quantum technologies [2–4]. Diamond coatings significantly enhance device performance and durability, particularly in harsh environments and high-temperature applications that demand superior resilience [5]. Moreover, integrating diamond materials in Micro-Electro-Mechanical Systems enables the development of advanced sensors, actuators, and other microscale devices with improved reliability and functionality [6,7].

The fabrication of micron-sized patterns in diamond films is crucial for high-tech applications and industries. However, achieving precise bulk patterning remains challenging due to the diamond's exceptional hardness and chemical inertness, which make traditional machining methods ineffective. Various post-growth processing techniques have been investigated for diamond film manipulation, including ion beam irradiation [8], laser etching and cutting [9], and reactive ion etching with O₂ or CF₄ plasma [10–12]. Although dry etching processes show promise, their effectiveness is often limited by mask material re-sputtering and the high costs of vacuum equipment for these processes.

Complementary to dry etching processes, temperature-accelerated chemical treatment techniques are well adopted in polishing treatments. The hot metal lapping technique, leveraging carbon's solubility in iron at elevated temperatures, enables high-quality polishing of rough diamond films. However, creating high-resolution structures requires reducing metal pattern thickness to the micrometer scale, which is challenging due to thin films' limited carbon dissolution capacity [13]. To

address this limitation, researchers have proposed treating diamond-metal systems through annealing in H_2 [13–15] or water vapor [16–18] rather than in vacuum or inert gas atmospheres. These environments promote mainly sp^2 carbon desorption from the metal surface, enabling continuous removal of dissolved carbon and accelerating diamond catalytic etching rates. This thermochemical reaction approach has been successfully demonstrated with various transition metals (Fe, Ni, Co, Ti) for diamond etching and patterning in mechanical machining applications [13,14].

Ni-catalyzed thermal graphitization of diamond presents both challenges and opportunities in transforming diamond into sp^2 -carbon form [14,19,20]. This process in high-temperature water vapor conditions enables deep etching, reaching hundreds of micrometers in monocrystalline diamond [17]. However, information on the etching of thick polycrystalline diamond films of randomly oriented microcrystals is lacking.

In this study, the potential for deep etching of thick polycrystalline diamond layers through catalytically driven reactions at high temperatures, using hydrogen (H_2) and/or carbon dioxide (CO_2) gas mixtures excited in microwave plasma, as well as a plasma-free environment in hydroxyl-rich water vapor (OH), is explored. The research focuses on optimizing key process parameters, including water vapor pressure, temperature, and process duration for Ni-catalyzed etching of microcrystalline diamond layers, aiming to achieve rapid and precise patterning.

2. Experimental

Microcrystalline diamond (MCD) layers were deposited on silicon substrates using microwave plasma-enhanced chemical vapor deposition (MW-PECVD). Before deposition, the silicon substrates were ultrasonically cleaned in acetone, isopropyl alcohol, and deionized water for 10 minutes each. To promote diamond nucleation, the substrates were treated in an aqueous suspension of nanodiamond powder (NanoAmando, 5 nm particle size) under ultrasonic agitation for 40 minutes [21].

The MCD layers were deposited using the MW-PECVD system (Seki Diamond Systems, SDS6K). Morphological analysis of the MCD films was performed with field emission scanning electron microscopy (SEM, Tescan Maia 3). SEM provided high-resolution imaging of surface features, grain boundaries, and crystal orientation. The microscope was operated at an acceleration voltage of 10 kV with a working distance of 2–5 mm to optimize image quality.

The MCD layer, shown in Fig. 1a, was synthesized under the following process parameters: a deposition duration of 5 hours, chamber pressure of 120 mbar, microwave power of 5 kW, and a gas mixture of 500 sccm hydrogen with 25 sccm methane. The average deposition temperature was kept at $960 \pm 20^\circ C$, resulting in a diamond layer thickness of approximately 10 μm .

After deposition, Ni strips with thicknesses of 50 nm and 200 nm were thermally evaporated onto the MCD surface using mechanical masks, as illustrated in Fig. 1b. The Ni strips were 150 μm wide, with 500 μm spacing between them.

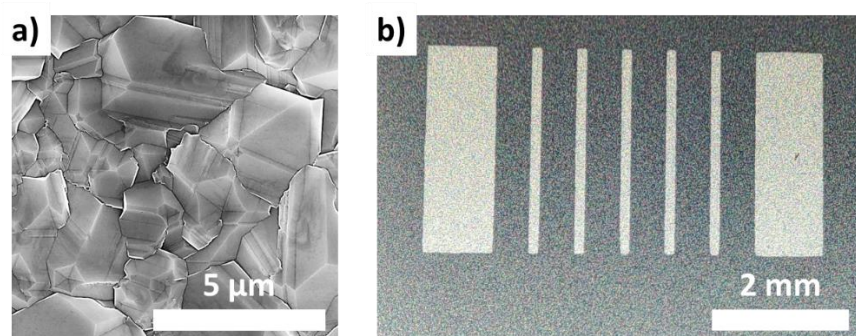


Fig. 1. (a) SEM photographs of the surface morphology of the prepared 10 μm MCD diamond layer; (b) Ni strips 200 nm evaporated on the MCD through the mechanical mask.

The MCD diamond samples covered with the evaporated Ni strips were exposed to water vapor (wet) annealing, as shown in Fig. 2 [16]. The annealing process was conducted under varying pressures ranging from 65 mbar to atmospheric pressure (1 bar). Nitrogen gas was bubbled through ultrapure demineralized water and introduced into an electric cylindrical furnace (CLASIC Ltd.) consisting of a quartz tube, resistive heating elements, and a ceramic holder.

The annealing temperature was maintained between 750°C and 975°C for 10 to 60 minutes. The nitrogen gas flow rate was regulated at 750 sccm throughout the process to ensure consistent reaction conditions.

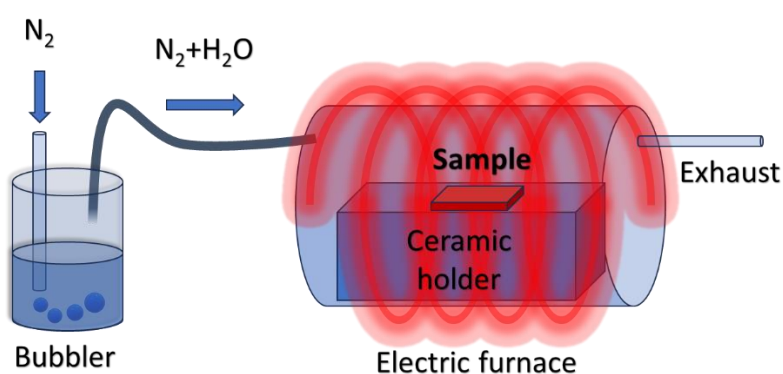


Fig. 2. Schematic side view of the water vapor annealing system.

3. Results and discussion

This section presents the experimental findings on the deep etching of microcrystalline diamond using H_2 and O_2 plasma, as well as hydroxyl-rich water vapor at elevated temperatures.

3.1 Etching diamond through Ni mask using H_2 and O_2 gases in MW plasma

Firstly, we investigated the impact of H_2 and O_2 -containing gas mixtures excited by plasma on Ni-catalyzed deep etching of MCD films. The experiments employed the same MW-PECVD apparatus used for diamond deposition, with the following parameters: chamber pressure of 120 mbar, microwave power of 5 kW, H_2 gas flow rate of 200 sccm and a substrate temperature of 900°C. These conditions were chosen with respect to a previous study on reactive molecular dynamics presented by Xu et al., who provide a comprehensive account of the mechanisms underlying the different etching of diamonds by H_2 and O_2 plasma [11].

When subjected to H_2 plasma etching with a 50 nm thick Ni mask, the MCD film showed minimal etching, as seen in Fig. 3a-c. Fig. 3a provides a top view of the MCD film post- H_2 plasma etching. Typically, H_2 plasma for 30 minutes does not etch diamond [22]; however, a slight surface etching of about 40-60 nm was observed, attributed to the gentle de-sputtering of the masking Ni layer onto the unmasked MCD regions. Fig. 3b shows a cross-sectional view of the MCD layer in the Ni-masked region after H_2 plasma etching, demonstrating negligible impact, with the original 10 μm thickness remaining unchanged. A detailed top view of the Ni-covered region after H_2 plasma etching is presented in Fig. 3c, revealing a slightly more pronounced etching of approximately 200 nm due to the higher Ni presence. So, these initial attempts with H_2 plasma are ineffective and lack selectivity. As the next, we introduced CO_2 (20 sccm, 10%) into the gas mixture to enhance etching efficiency. Fig. 3d illustrates a 45° angled view of the MCD film post- O_2 plasma etching, highlighting increased surface changes. The cross-sectional view (Fig. 3e) revealed almost 2.5 μm etching of diamond from the unmasked MCD film after 30 minutes. Fig. 3f displays a detailed top view of the Ni-masked MCD film, revealing an inhomogeneous etching with Ni clusters embedded about 1 μm into the MCD film. The addition of CO_2 substantially increased the etching rate; however, it also resulted in non-selective

etching, affecting both masked and unmasked areas. Given the limitations of H_2 and O_2 plasma etching, we changed process parameters to high-temperature water vapor (OH) etching, inspired by a recent study on single-crystal diamond etching with water vapor [17].

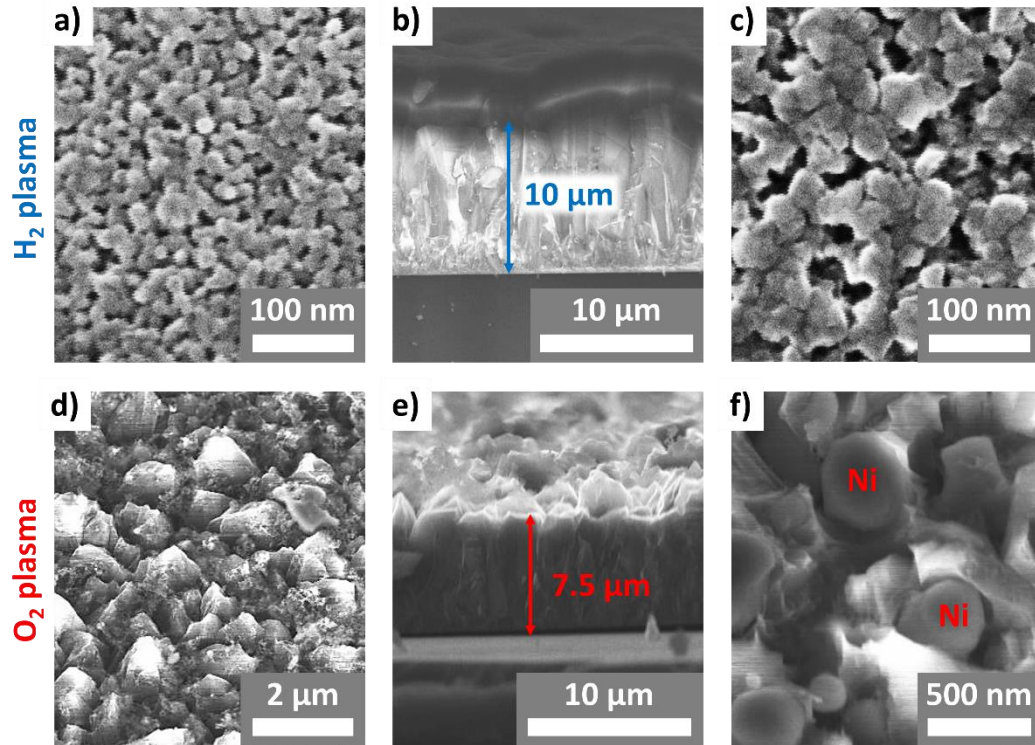


Fig. 3: SEM images illustrating various stages of the MCD film MW plasma etching process: (a) top view of the MCD film post- H_2 plasma treatment; (b) cross-sectional view of the MCD film after H_2 plasma etching in the Ni-masked region; (c) top view of the Ni-masked area of the MCD film post- H_2 plasma treatment; (d) 45° angled view of the MCD film following O_2 plasma etching; (e) cross-sectional view of the MCD film after O_2 plasma etching; (f) top view of the Ni-masked area of the MCD film post- O_2 plasma treatment.

3.2 Impact of pressure and Ni thickness

Under low-pressure conditions (65 mbar) in a water vapor-enriched environment at 900°C for 30 minutes, etching pits up to 5 μm was achieved in the diamond layer using a thin 50 nm Ni mask (Fig. 4a). However, the process was abruptly hindered due to the rapid graphitization of the diamond (i.e., sp^2 hybridization), which restricted the sp^2 carbon removal by hydroxyl radicals. Keeping process parameters constant, only raising the OH pressure to atmospheric level (1 bar) resulted in the etching pits 8 μm on average (see Fig. 4b). To enhance the relatively low etching efficiency MCD films with 50 nm Ni mask, we further increased its thickness. Utilizing a 200 nm-thick Ni layer, the diamond beneath Ni was planarly etched through the entire thickness of 10 μm (Fig. 4c). Other possibilities how to enhance the etching efficiency is an increase of temperature up to 975°C while keeping the initial Ni mask at 50 nm. It was found that the diamond was also entirely etched down to the substrate, exposing its surface within just 15 minutes, as shown in Fig 4d.

We can conclude that the water vapor etching process conditions demonstrate high selectivity, leaving unmasked diamond regions completely intact and unaffected. Moreover, the etching provided at the lower temperature of 900°C and thicker Ni layer (200 nm) is comparable to the process done at higher temperature (975°C) and thinner Ni (50 nm). This selectivity is clearly illustrated in Fig. 4c-d, where unmasked regions of the diamond remained entirely unaltered for both processes.

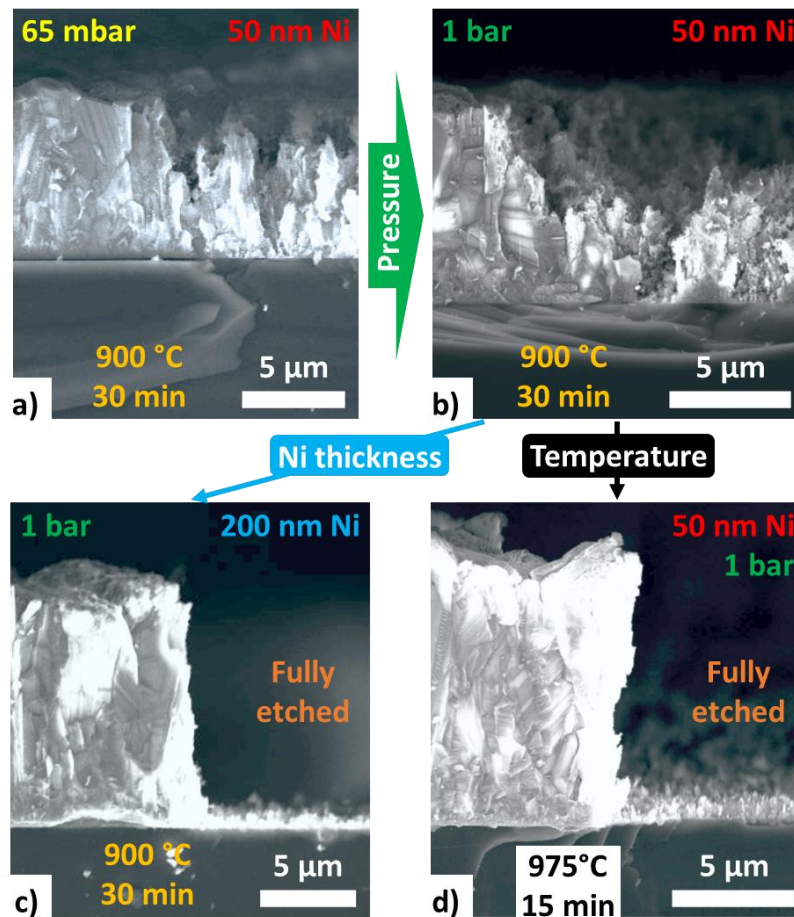


Fig. 4. SEM images of the impact of pressure and Ni thickness show the structured 10 μm MCD after etching: (a) cross-section view with 50 nm Ni at low-pressure 65 mbar at 900°C for 30 minutes; (b) cross-section view with 50 nm Ni at atmospheric pressure 1 bar at 900°C for 30 minutes; (c) cross-section view with four-fold increase of Ni thickness, 200 nm Ni at atmospheric pressure 1 bar at 900°C for 30 minutes; (d) cross-section view with 50 nm Ni at atmospheric pressure 1 bar at 975°C for 15 minutes.

3.3 Effect of temperature

The next series of experiments focused on studying the impact of temperature ranging from 750°C to 900°C on the etching of MCD films at atmospheric pressure in water vapor conditions. This involved depositing a 200 nm Ni layer onto a 20 μm thick MCD substrate grown for 10 hours under the same conditions as the initial one (with a thickness of 10 μm). The etching time was 1 hour for all samples. The cross-section views of the etching profiles of the MCD layers are summarized in Fig. 5. At 750°C, the etching depth is as low as 2 μm. Raising the temperature to 800°C, the etching rate rose almost twice, resulting in a depth of 5 μm. Above 800°C, the etching depth steadily increased to 15 μm (850°C), and full etching of the MCD layer characterized by nearly vertical sidewalls down to the Si substrate was observed at 900°C. While the MCD film was promptly etched at 900°C, we shortened the etching process to 10 minutes. The etched depth was 8 μm (Fig. 6a), indicating the etching rate was higher than 45 μm/h. Fig. 6b plots the dependence of the calculated etch rate on the temperature.

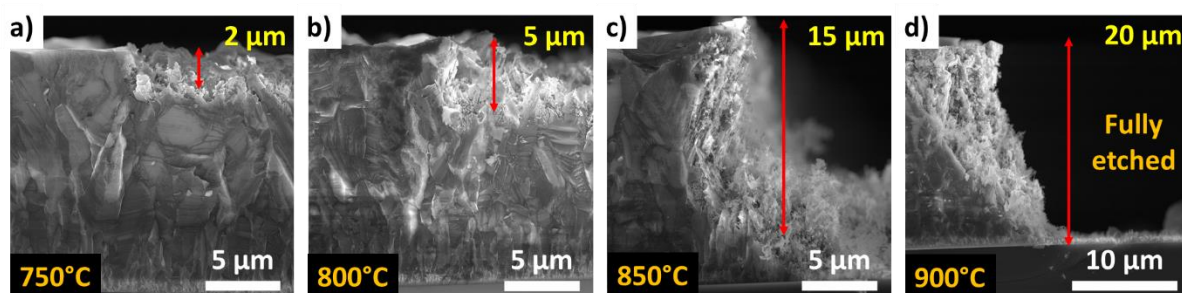


Fig. 5. Cross-section SEM images of MCD films treated at different temperatures: (a) 750°C; (b) 800°C; (c) 850°C; (d) 900°C. The MCD films were 20 μm thick and annealed for 1 hour at the given temperature.

Fig. 6c shows the Raman spectrum of the MCD sample etched for 10 minutes at two distinct regions: the unmasked and Ni-masked areas. Both spectra are dominated by two sharp peaks centered at 520 cm^{-1} , the silicon substrate, and 1333 cm^{-1} attributed to the sp^3 -bonded carbon in diamond. After the etching process, the MCD film from the masked area revealed a band at approx. 1394 cm^{-1} , which should be assigned to sp^2 hybridized carbon forms or partially disordered carbon in sp^3 clusters [19], suggesting etching-induced graphitization of the diamond phase. Moreover, the interaction between Ni and the diamond surface might also influence the local vibrational modes, leading to the observed spectral changes [23–25].

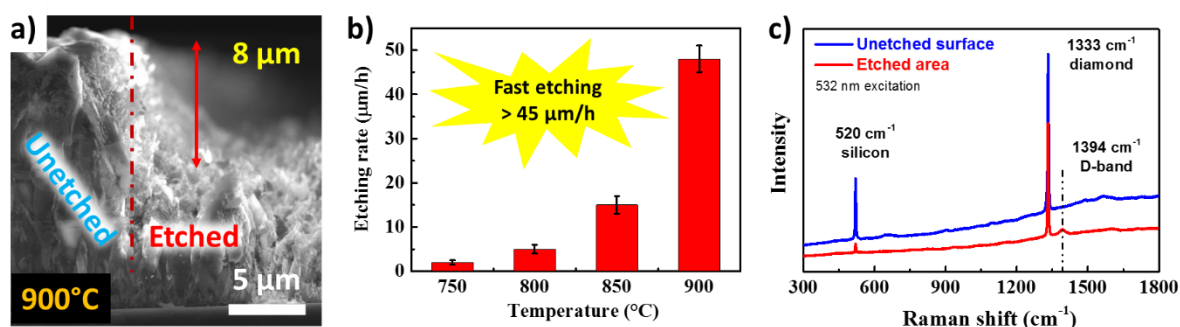


Fig. 6. (a) SEM image after 10 minutes etching of 20 μm MCD at 900°C; (b) etching rate of MCD film through 200 nm Ni layer at different temperatures; (c) Raman spectra after etching from the unmasked (unetched) and Ni-masked (etched) areas.

These experiments demonstrate that highly anisotropic etching could be achieved with a certain degree of vertical sidewalls, which represents a valuable process advancement. It offers strict control over feature geometry compared to the sloped profiles, as observed in single-crystal diamond etching presented by Nagai et al. [17]. They reported analogous anisotropic etching patterns in single crystalline diamond, similar to those observed in silicon, resulting in distinctive truncated inverted pyramidal structures. The angle between the four side walls and (100) planes was approximately 55°, which corresponds to the crystallographic angle between the {111} and (100) planes, demonstrating the strong influence of crystal orientation on the etching process. Our experiments suggest that the etching mechanism might be less dependent on the diamond crystal orientation and more sensitive to the process parameters once the process parameters are optimized (i.e., Ni thickness, temperature, pressure).

3.4 Schematic model of thermochemical etching

Nagai et al. proposed a model explaining the diamond etching mechanism through water vapor, which promotes and accelerates diamond graphitization [17]. We have extended this model by establishing

correlations between process parameters and etching profiles in polycrystalline diamond films in terms of etching anisotropy/selectivity. The proposed model is schematically shown in Fig. 7.

In agreement with Nagai, water vapor provides OH radicals while the Ni catalytic function is activated by the mutual influence of pressure and temperature. We previously observed [19] that the disordered carbon initially forms at the Ni-diamond interface under elevated temperatures, which is then progressively transformed into the graphitic phase. The sp^2 -hybridized carbon species diffuse through and around the Ni layer or particles, respectively, leading to increased carbon concentration both within Ni and at its top surface.

Here, the reaction can slow down (nearly stop) when a critical concentration of accumulated sp^2 carbon is achieved, resulting in low etching efficiency at low pressures (Fig. 7b). However, increasing water vapor pressure from 65 mbar to 1 bar retrieves the catalytic dissolving of the diamond by removing saturated sp^2 carbon atoms from the Ni top surface (Fig. 7c). The sp^2 carbon removal from Ni interface is thermally amplified, as well as carbon diffusion and overall graphitization. Consequently, high-temperature conditions result in fast etching rates of diamond ($>45 \mu\text{m/h}$). In analogy to that, an increase in the Ni thickness can further positively influence the etching efficiency by prolonging the time period required for the sp^2 carbon saturation in and around the Ni mask (Fig. 7d).

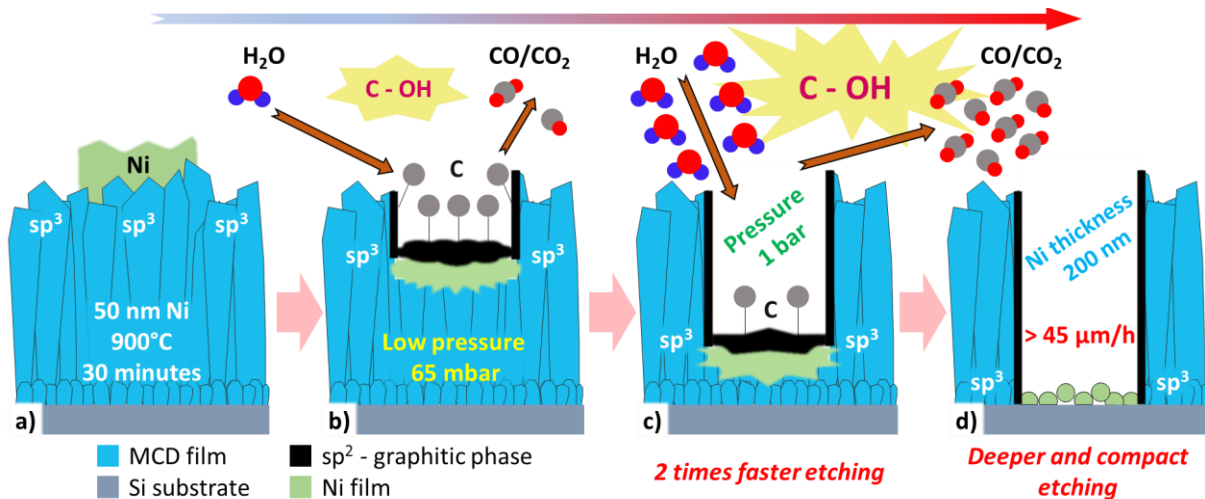


Fig. 7. Schematic model of the catalytic etching of diamond layers accelerated by water vapor with the presence of Ni particles as a function of pressure, temperature, and Ni thickness.

4. Conclusions

In conclusion, we extended a thermochemical etching methodology for polycrystalline diamond films using Ni as a catalyst. The developed mechanism demonstrates that the synergistic effect of water vapor pressure, temperature, and Ni catalyst thickness critically influences the etching kinetics and profile characteristics. Under optimized conditions (atmospheric pressure, 900°C, 200 nm Ni mask thickness), the process achieved significant etching rates exceeding 45 $\mu\text{m/h}$ while maintaining vertical sidewall profiles and high selectivity, effectively preserving unexposed diamond regions while completely removing Ni-masked areas.

This methodology offers a viable alternative to conventional plasma-based dry etching processes, particularly for fabricating high-aspect-ratio structures such as deeply embedded electrodes and complex architectures in various applications, including diamond-based 3D dosimeters, neural interfaces, biosensors, and energy storage devices. The demonstrated results suggest that careful control of process parameters is essential for optimizing etching performance and achieving desired structural outcomes.

Acknowledgments

This work was supported by the Ministry of Education, Youth and Sports of the Czech Republic, grant No. LUASK22147 (SK no SK-CZ-RD-21-0116). We acknowledge CzechNanoLab Research Infrastructure supported by MEYS CR (LM2023051) and the OP JAC financed by ESIF and the MEYS SENDISO—CZ.02.01.01/00/22_008/0004596. The authors kindly thank Rajisa Jackivová and Karel Hruška for SEM measurements and Zuzana Gedeonová for the evaporation of Ni strips.

Data availability

The data that support the findings of this study are openly available at <https://doi.org/10.5281/zenodo.14638241>.

References

- [1] R.S. Sussmann, ed., CVD diamond for electronic devices and sensors, J. Wiley, Chichester, U.K, 2009.
- [2] I. Aharonovich, A.D. Greentree, S. Praver, Diamond photonics, *Nat. Photonics* 5 (2011) 397–405. <https://doi.org/10.1038/nphoton.2011.54>.
- [3] A.D. Greentree, B.A. Fairchild, F.M. Hossain, S. Praver, Diamond integrated quantum photonics, *Mater. TODAY* 11 (2008) 22–31. [https://doi.org/10.1016/S1369-7021\(08\)70176-7](https://doi.org/10.1016/S1369-7021(08)70176-7).
- [4] M. Radulaski, J.L. Zhang, Y. Tzeng, K.G. Lagoudakis, H. Ishiwata, C. Dory, K.A. Fischer, Y.A. Kelaita, S. Sun, P.C. Maurer, K. Alassaad, G. Ferro, Z. Shen, N.A. Melosh, S. Chu, J. Vučković, Nanodiamond Integration with Photonic Devices, *Laser Photonics Rev.* 13 (2019) 1800316. <https://doi.org/10.1002/lpor.201800316>.
- [5] V. Shanov, R.N. Singh, W. Tabakoff, CVD diamond coating for erosion protection at elevated temperatures, *J. Mater. Eng. Perform.* 11 (2002) 220–225. <https://doi.org/10.1361/105994902770344303>.
- [6] E. Kohn, P. Gluche, M. Adamschik, Diamond MEMS — a new emerging technology, *Diam. Relat. Mater.* 8 (1999) 934–940. [https://doi.org/10.1016/S0925-9635\(98\)00294-5](https://doi.org/10.1016/S0925-9635(98)00294-5).
- [7] M.A. Huff, D.A. Aidala, J.E. Butler, MEMS applications using diamond thin films, *Solid State Technol.* 49 (2006) 45–46.
- [8] G. García, I. Preda, M. Díaz-Híjar, V. Tormo-Márquez, O. Peña-Rodríguez, J. Olivares, F. Bosia, N.M. Pugno, F. Picollo, L. Giuntini, A. Sordini, P. Olivero, L. López-Mir, C. Ocal, Micro and nano-patterning of single-crystal diamond by swift heavy ion irradiation, *Diam. Relat. Mater.* 69 (2016) 1–7. <https://doi.org/10.1016/j.diamond.2016.06.015>.
- [9] M.C. Polo, J. Cifre, G. Sánchez, R. Aguiar, M. Varela, J. Esteve, Pulsed laser deposition of diamond from graphite targets, *Appl. Phys. Lett.* 67 (1995) 485–487. <https://doi.org/10.1063/1.114544>.
- [10] A. Toros, M. Kiss, T. Graziosi, S. Mi, R. Berrazouane, M. Naamoun, J. Vukajlovic Plestina, P. Gallo, N. Quack, Reactive ion etching of single crystal diamond by inductively coupled plasma: State of the art and catalog of recipes, *Diam. Relat. Mater.* 108 (2020) 107839. <https://doi.org/10.1016/j.diamond.2020.107839>.
- [11] J. Xu, K. Lu, D. Fan, Y. Wang, S. Xu, M. Kubo, Different Etching Mechanisms of Diamond by Oxygen and Hydrogen Plasma: a Reactive Molecular Dynamics Study, *J. Phys. Chem. C* 125 (2021) 16711–16718. <https://doi.org/10.1021/acs.jpcc.1c03919>.
- [12] T. Ižák, O. Szabó, P. Štenclová, Š. Potocký, V. Vyskočil, A. Kromka, Fabrication of Structured Boron-Doped Diamond Films for Electrochemical Applications, *Proceedings* 2 (2018) 984. <https://doi.org/10.3390/proceedings2130984>.
- [13] V.G. Ralchenko, T.V. Kononenko, S.M. Pimenov, N.V. Chernenko, E.N. Loubnin, V.Yu. Armejev, A.Yu. Zlobin, Catalytic interaction of Fe, Ni and Pt with diamond films: patterning applications, *Diam.* 1992 2 (1993) 904–909. [https://doi.org/10.1016/0925-9635\(93\)90248-Z](https://doi.org/10.1016/0925-9635(93)90248-Z).
- [14] H. Aida, K. Ikejiri, S.-W. Kim, K. Koyama, Y. Kawamata, H. Kodama, A. Sawabe, Overgrowth of diamond layers on diamond microneedles: New concept for freestanding diamond substrate by

- heteroepitaxy, *Diam. Relat. Mater.* 66 (2016) 77–82.
<https://doi.org/10.1016/j.diamond.2016.03.019>.
- [15] H. Mehedi, J.-C. Arnault, D. Eon, C. Hébert, D. Carole, F. Omnes, E. Gheeraert, Etching mechanism of diamond by Ni nanoparticles for fabrication of nanopores, *Carbon* 59 (2013) 448–456.
<https://doi.org/10.1016/j.carbon.2013.03.038>.
- [16] R. Yoshida, D. Miyata, T. Makino, S. Yamasaki, T. Matsumoto, T. Inokuma, N. Tokuda, Formation of atomically flat hydroxyl-terminated diamond (1 1 1) surfaces via water vapor annealing, *Appl. Surf. Sci.* 458 (2018) 222–225. <https://doi.org/10.1016/j.apsusc.2018.07.094>.
- [17] M. Nagai, K. Nakanishi, H. Takahashi, H. Kato, T. Makino, S. Yamasaki, T. Matsumoto, T. Inokuma, N. Tokuda, Anisotropic diamond etching through thermochemical reaction between Ni and diamond in high-temperature water vapour, *Sci. Rep.* 8 (2018) 6687.
<https://doi.org/10.1038/s41598-018-25193-2>.
- [18] B.P. Payne, M.C. Biesinger, N.S. McIntyre, The study of polycrystalline nickel metal oxidation by water vapour, *J. Electron Spectrosc. Relat. Phenom.* 175 (2009) 55–65.
<https://doi.org/10.1016/j.elspec.2009.07.006>.
- [19] O. Romanyuk, M. Varga, S. Tulic, T. Izak, P. Jiricek, A. Kromka, V. Skakalova, B. Rezek, Study of Ni-Catalyzed Graphitization Process of Diamond by in Situ X-ray Photoelectron Spectroscopy, *J. Phys. Chem. C* 122 (2018) 6629–6636. <https://doi.org/10.1021/acs.jpcc.7b12334>.
- [20] S. Tulić, T. Waitz, M. Čaplovičová, G. Habler, M. Varga, M. Kotlár, V. Vretenár, O. Romanyuk, A. Kromka, B. Rezek, V. Skákalová, Covalent Diamond–Graphite Bonding: Mechanism of Catalytic Transformation, *ACS Nano* 13 (2019) 4621–4630. <https://doi.org/10.1021/acsnano.9b00692>.
- [21] A. Kromka, B. Rezek, Z. Remes, M. Michalka, M. Ledinsky, J. Zemek, J. Potmesil, M. Vanecek, Formation of Continuous Nanocrystalline Diamond Layers on Glass and Silicon at Low Temperatures, *Chem. Vap. Depos.* 14 (2008) 181–186. <https://doi.org/10.1002/cvde.200706662>.
- [22] H. Jiang, F. Liu, H. Yan, L. Si, Z. Dou, Etching effects of hydrogen plasma treatment on diamond surfaces, *Surf. Coat. Technol.* 363 (2019) 12–17. <https://doi.org/10.1016/j.surfcoat.2019.02.007>.
- [23] W.-T. Huang, C. Lin, X. Li, J. Zang, L. Wan, Z. Zhang, S. Cheng, C. Shan, Influence of structural defects toward the nickel-catalyzed etching behaviors of synthetic diamond, *Acta Mater.* 263 (2024) 119527. <https://doi.org/10.1016/j.actamat.2023.119527>.
- [24] A. Dychalska, W. Koczorowski, M. Trzcinski, L. Mosińska, M. Szybowicz, The Effect of Surface Treatment on Structural Properties of CVD Diamond Layers with Different Grain Sizes Studied by Raman Spectroscopy, *Materials* 14 (2021) 1301. <https://doi.org/10.3390/ma14051301>.
- [25] R. Carcione, E. Tamburri, R. Bartali, G. Speranza, V. Micheli, G. Pepponi, P. Bellutti, M.L. Terranova, On the route to produce conductive Ni-related color centers in CVD-grown diamond, *Multifunct. Mater.* 2 (2019) 035001. <https://doi.org/10.1088/2399-7532/ab2c35>.